Minimal Membrane Interactions Conferred by Rheb C-terminal Farnesylation are Essential for mTORC1 Activation

Brittany Angarola[1,2], and Shawn M. Ferguson[1,2*]

Departments of Cell Biology and Neuroscience[1], Program in Cellular Neuroscience, Neurodegeneration and Repair[2], Yale University School of Medicine, New Haven, CT, 06510

[*]To whom correspondence should be addressed

e-mail: shawn.ferguson@yale.edu

phone: 203-737-5505

fax: 203-737-2065

Abstract

Stable localization of the Rheb GTPase to lysosomes is thought to be required for activation of mTORC1 signaling. However, the lysosome targeting mechanisms for Rheb remain unclear. We therefore investigated the relationship between Rheb subcellular localization and mTORC1 activation. Surprisingly, we found that although Rheb was prominently enriched at the endoplasmic reticulum (ER), Rheb was undetectable at lysosomes. Functional assays in knockout human cells revealed that farnesylation of the C-terminal CaaX motif on Rheb was essential for both Rheb enrichment on ER membranes and mTORC1 activation. However, constitutively targeting Rheb to ER membranes did not support mTORC1 activation. Further systematic analysis of the Rheb hypervariable region revealed that weak, non-selective, farnesylation-dependent, membrane interactions confer Rheb function without the need for a specific lysosome targeting motif. Collectively, these results argue against stable interactions of Rheb with lysosomes and instead that transient membrane interactions optimally allow Rheb to activate mTORC1 signaling.

Introduction

The mTOR complex 1 (mTORC1) signaling pathway plays a major role in matching cell growth and metabolism to ongoing changes in environmental conditions. Multiple signals converge on the surface of lysosomes to regulate the activity of the Rag and Rheb small GTPases that recruit and activate mTORC1 respectively. This has led to a widely accepted two step model for mTORC1 activation wherein Rags recruit mTORC1 to lysosomes followed by Rheb-dependent activation of mTORC1 kinase activity (Fig. S1A) (Ben-Sahra and Manning, 2017; Ferguson, 2015; Sancak et al., 2008; Saxton and Sabatini, 2017). However, even though farnesylation at its C-terminus has been widely accepted as a means of localizing Rheb to lysosomes, there is only limited direct support for this (Menon et al., 2014; Sancak et al., 2010; Sancak et al., 2008) and the underlying mechanism is vague as a farnesyl group is only expected to confer weak membrane interactions and has no innate selectivity for binding to lysosomes over other organelles (Silvius et al., 2006; Silvius and l'Heureux, 1994). Adding to the confusion, it has recently alternatively been proposed that Rheb instead localizes to either the ER or Golgi and activates mTORC1 via contact sites between these organelles and lysosomes (Hao et al., 2018; Walton et al., 2018).

To address the problem of where Rheb functions and the mechanisms that target Rheb to its subcellular site of action, we systematically investigated the relationship between Rheb localization and function in human cells. Surprisingly, our data indicates that Rheb does not require stable enrichment on a specific organelle. Instead, weak membrane interactions conferred by Rheb farnesylation Rheb are a positive feature that is essential for mTORC1 activation.

Results and Discussion

Rheb is not enriched on the surface of lysosomes. In contrast to the previously reported localization of Rheb to LAMP1-positive lysosomes in HeLa cells (Menon et al., 2014), we found that Rheb showed no major enrichment on such organelles (Fig. 1A), even though we used the same combination of antibody for Rheb detection and Rheb siRNA for verifying signal specificity (Fig. 1B). This difference in conclusions arises mainly from improved preservation and more stringent criteria for overcoming the challenge of interpreting the broad intracellular distribution of Rheb. As the Rheb protein is widely distributed throughout cells, some Rheb inevitably overlaps with the LAMP1 signal. However, our analysis of the colocalization between Rheb and LAMP1 revealed that the degree of overlap between these two proteins was no greater than chance (Fig. 1C). As a control for the Rheb siRNA, immunoblotting experiments confirmed Rheb depletion following Rheb siRNA transfection and demonstrated that mTORC1 signaling was suppressed in these cells (Fig S1B-S1D).

As mTOR and many mTORC1 regulatory proteins exhibit dynamic changes in their levels at lysosomes in response to acute changes in amino acid availability [Fig. S1A; (Saxton and Sabatini, 2017)], we next examined the effect of amino acid starvation and re-feeding on Rheb localization. In contrast to mTOR, which was found throughout the cytosol under starved conditions but underwent a robust increase in its recruitment to lysosomes in response to amino acid re-feeding, Rheb localization was not responsive to such stimuli and failed to co-enrich with mTOR puncta even though mTORC1 signaling was stimulated in response to the amino acid re-feeding (Fig. S1E-S1G).

To generate an alternative tool for detecting the endogenous Rheb protein, we used CRISPR-Cas9 gene editing to insert a 2xHA epitope tag immediately downstream of the

start codon in the endogenous Rheb locus in HeLa cells (Fig. S2A and S2B). However, the anti-HA immunofluorescence still did not show enrichment on lysosomes in these cells (Fig. 1D and 1E).

Live cell imaging detects enrichment of GFP-Rheb at the endoplasmic reticulum. As preserving Rheb on lysosomes could require specialized fixation, permeablization and/or antibody incubation conditions, we next examined the localization of GFP-tagged Rheb in live HeLa cells and observed a combination of cytosolic and endoplasmic reticulum (ER)-like localization pattern (Fig. 2A). Rheb localization was further investigated in COS-7 cells as they contain a well-defined peripheral ER network that is highly suitable for live cell imaging studies (Fig. 2B) (Rowland et al., 2014). In addition to colocalizing extensively with mRFP-Sec61 (an ER protein), there was also a diffuse pool of Rheb in the cytosol (Fig. 2C). In contrast, GFP-Rheb and LAMP1-mCherry (lysosome marker) had distinct, non-overlapping, patterns of subcellular distribution. Interestingly, even though Rheb was not enriched on lysosomes, lysosomes were frequently adjacent to Rheb-positive ER tubules (Fig. 2D, Movie S1).

Knockout cells reveal redundant functions for Rheb and RhebL1. In order to directly test the relationship between Rheb subcellular localization and function, we used CRISPR-Cas9 genome editing to mutate both Rheb and the closely related RhebL1 genes in Hela cells and isolated a clonal population of cells that contained mutations at the target sites in both genes (Fig S2C). Although Rheb protein levels were undetectable in these cells, basal levels of mTORC1 signaling were near normal (Fig. 3A and 3B). As one of the three Rheb mutant alleles contained an in frame 6 bp deletion (Fig S2B), we suspected that traces of this mutant Rheb protein might support physiologically significant levels of Rheb function. Indeed, treating the Rheb+RhebL1 mutant cells with Rheb siRNA resulted in near complete suppression of basal mTORC1 signaling (Fig. 3A

and 3B; S2D and S2E). In light of these observations, we will subsequently refer to the Rheb+RhebL1 genomic mutant cell line as “Edited” and the cells that have additionally been treated with Rheb siRNA as “Depleted”.

Rheb C-terminal farnesylation is essential for mTORC1 signaling and Rheb localization to the ER. mTORC1 signaling (S6K-T389 phosphorylation) was restored following expression of either GFP-Rheb or GFP-RhebL1 in $Rheb^{Depleted}$ cells (Fig. 3C and 3D). Similar to GFP-Rheb, GFP-RhebL1 exhibited an ER-like localization pattern (Fig. 3G, S3A and B). Both Rheb and RhebL1 contain a C-terminal CaaX motif (cysteine followed by 2 aliphatic amino acids and X in the final position) wherein the cysteine is farnesylated (Fig. 4A; (Clark et al., 1997). A Rheb mutant that lacked the CaaX motif, was unable to rescue mTORC1 activity in $Rheb^{Depleted}$ cells (Fig. 3C and 3D) and exhibited a diffuse subcellular distribution (Fig. 3F). These results indicate that Rheb cannot efficiently activate mTORC1 signaling from the cytosol and that farnesylation-dependent membrane interactions are essential for its function. This interpretation is corroborated by previous in vitro experiments that ruled out a direct role for Rheb farnesylation in mTORC1 activation that is distinct from its role in regulating membrane interactions of Rheb (Sato et al., 2009).

Following the cytosolic farnesylation reaction, Rheb is further processed at the endoplasmic reticulum by Ras converting enzyme (RCE1) and isoprenylcysteine carboxymethyltransferase (ICMT) (Takahashi et al., 2005). However, the ER localization of Rheb does not predominantly reflect processing of newly synthesized Rheb as treatment of cells with cycloheximide to block new protein synthesis did not reduce Rheb abundance at the ER (Fig. S4).

Constitutive ER localization of Rheb does not support mTORC1 signaling. The prominent membrane contact sites between ER and lysosomes suggested that ER-

localized Rheb might reach across such regions of proximity to activate mTORC1 that has been recruited to lysosomes via interactions with the Rags (Walton et al., 2018). To test this model, we generated a chimeric protein comprised of GFP-Rheb$^{\Delta CaaX}$ fused to the transmembrane domain of cytochrome B5 (Fig. 3H), a well-established ER targeting signal (Honsho et al., 1998). This chimeric protein localized to the ER (Fig 3I) but did not restore mTORC1 activity in Rheb^{Depleted} cells (Fig. 3J and 3K) even though we still observed frequent contact between ER and lysosomes in cells expressing GFP-Rheb-ER (Fig. 3L). As neither the completely cytosolic Rheb$^{\Delta CaaX}$ mutant nor the constitutively ER-targeted Rheb mutant were functional, we next focused more intensely on the role played by Rheb farnesylation and the possibility of additional regulation conferred by nearby sequences in the Rheb C-terminal hypervariable region.

Rheb C-terminal farnesylation supports mTORC1 signaling without any requirement for additional targeting motifs in the surrounding hypervariable region. In contrast to Rheb and RhebL1 whose ER and cytosolic localization is seemingly at odds with their ability to activate mTORC1 on lysosomes, other members of the Ras superfamily such as H-Ras localize robustly to their major site of action at the plasma membrane (Choy et al., 1999; Hancock et al., 1990). The plasma membrane localization of H-Ras depends on C-terminal farnesylation accompanied by 2 additional cysteine residues within the adjacent hypervariable region that are palmitoylated (Fig. 4A) (Choy et al., 1999; Hancock et al., 1990). It was also reported that the last 15 amino acids of Rheb acts as a lysosome targeting signal (Sancak et al., 2010). This suggested that this sequence should contain an additional determinant that cooperates with farnesylation to target Rheb to lysosomes.

To investigate the role of the CaaX motif and its flanking sequences in determining the subcellular localization and function of Rheb, we generated a chimera wherein the Rheb

C-terminus was replaced with the last 20 amino acids from H-Ras. This Rheb-H-Ras protein localized robustly to the plasma membrane (Fig. 4B and 4C) and was less effective than full length Rheb at activating mTORC1 signaling (Fig. 4E and 4F). Although, H-Ras predominantly localizes to the plasma membrane, it is also undergoes cycles of depalmitoylation that allow it to transiently visit intracellular membranes in the farnesylated state (Rocks et al., 2005). To test the idea that farnesyaltion alone is the essential determinant of Rheb localization and function, we generated a mutant Rheb-H-Ras chimera that lacks the palmitoylated cysteines in the hypervariable region (Fig. 4A). This protein was no longer enriched at the plasma membrane; had a similar localization pattern to the WT Rheb (Fig. 4B and 4D); and promoted mTORC1 activity just as well as the WT GFP-Rheb (Fig. 4E and 4F). As Rheb, RhebL1 and the palmitoylation deficient H-Ras hypervariable regions lack sequence similarity beyond their CaaX motifs (Fig. 4A), these results indicate that farnesylation, independent from any other major determinants within the Rheb hypervariable region, is both necessary and sufficient for the ability of Rheb to interact with membranes and support mTORC1 signaling. Consistent with a model wherein Rheb C-terminal farnesylation only supports transient membrane interactions, subcellular fractionation revealed that Rheb was predominantly found in the cytosolic fraction and only minimally present in the membrane fraction (Fig. 4G).

Implications of weak Rheb membrane interactions for mTORC1 signaling. It is surprising that the minimal membrane targeting affinity and specificity of Rheb/RhebL1 optimally supports mTORC1 signaling as this stands in contrast to other members of the Ras superfamily that exhibit robust targeting to the membranes, where they in turn recruit their downstream effectors, However, there are several important factors that make Rheb distinct from other members of the Ras family. First, Rags, are responsible

for bringing mTORC1 to lysosomes when amino acids are abundant (Sancak et al., 2008; Saxton and Sabatini, 2017). In contrast, we demonstrated that Rheb is not required for mTOR enrichment on the surface of lysosomes (Fig. S2F). Thus, unlike other Ras family members, Rheb does not mediate membrane recruitment of downstream effectors and therefore does not require stable residence on lysosomes. Second, recent structures of Rheb-mTORC1 complexes revealed that Rheb stimulates mTORC1 catalytic activity by binding to mTOR and inducing a conformational change rearranges the mTOR kinase domain (Yang et al., 2017). Once this activation takes place, mTORC1 phosphorylates diverse substrates that reside throughout the cell (Ben-Sahra and Manning, 2017; Gonzalez and Hall, 2017; Saxton and Sabatini, 2017). Thus, the modest membrane affinity that is provided by Rheb farnesylation may represent an optimal solution for reducing dimensionality to facilitate interactions with lysosome-localized mTORC1 while also allowing the activated Rheb-mTORC1 complex to subsequently leave the lysosome to phosphorylate downstream targets that reside elsewhere in the cell. An additional layer of regulation conferred by Rheb C-terminal farnesylation arises through binding to PDEδ, and the actions of the Arl2 GTPase that releases prenylated cargos from PDEδ (Ismail et al., 2011; Zimmermann et al., 2013).

Conclusions. This study demonstrates that minimal membrane interactions conferred by Rheb C-terminal farnesylation optimally support mTORC1 signaling. This finding contrasts with previous models proposing that stable and specific association of Rheb with lysosomes or other organelles is essential for Rheb function. By overturning these widely held beliefs, our new findings will guide future studies that focus on understanding how dynamic Rheb membrane interactions are coordinated with the Rag-dependent localization of mTORC1 to lysosomes to activate mTORC1 signaling in health and disease.

Acknowledgements

This research was supported in part by grants from the NIH (GM105718) and the Ellison Medical Foundation to SMF. BA was supported by an NSF Graduate Research Fellowship (DGE1752134). Pamela Torola contributed to early phases of this project and Arun Tharkeshwar provided helpful advice related to cell fractionation. Microscopy studies were supported by the Yale University Program in Cellular Neuroscience, Neurodegeneration and Repair imaging facility.

Methods

Cell Culture and Transfection

HeLa M cells and COS7 cells (both provided by P. De Camilli, Yale University, New Haven) were grown in high-glucose Dulbecco's Modified Eagle's medium (DMEM) with L-glutamine, 10% fetal bovine serum, and 1% penicillin/streptomycin supplement (ThermoFisher Scientific, Waltham, MA and Corning, Corning, NY). To starve cells of amino acids, cells were incubated in amino acid-free RPMI media (US Biologicals, Swampscott, MA) for 2 hours. Cells were re-fed with RPMI containing 1X MEM amino acid supplement (Invitrogen) for 20 minutes.

To perform plasmid transfections, 500 ng of plasmid DNA, 1.5 µl of Fugene 6 transfection reagent (Promega, Madison, WI) and 100 µl of OptiMEM (ThermoFisher Scientific) were added to 80,000 cells per well in a 6-well dish. For siRNA transfections, 5 µl of RNAiMAX (ThermoFisher Scientific), 500 µl of OptiMEM and 5 µl of 20 µM siRNA stock were added to a subconfluent dish of cells (80,000 cells per well in a 6-well dish). Cells were incubated for 48 hours post-transfection prior to experiments. Control siRNA (5′-CGUUAAUCGCGUAUAAUACGCGUAT-3′) was purchased from Integrated DNA Technologies (IDT, Coralville, IA) and a previously described Rheb siRNA (Menon et al., 2014) was purchased from Cell Signaling Technology ((#14267, CST, Danvers, MA). Drugs utilized in this study: Cycloheximide (Millipore Sigma, Burlington, MA, #239765).

Plasmids

pRK5 plasmid encoding HA-GST human Rheb was acquired from D. Sabatini (Massachusetts Institute of Technology, Cambridge, MA) via Addgene (Plasmid #14951,

(Sancak et al., 2007)). Full length Rheb was PCR amplified from this vector and cloned into *SmaI*-digested pEGFPC1 by Gibson Assembly (New England Biolabs, Ipswich, MA). The Q5 Site-Directed Mutagenesis Kit (New England Biolabs) was used to generate GFP-Rheb$^{\Delta CAAX}$, GFP-Rheb-HRas, and GFP-Rheb-HRas$^{C\rightarrow A}$ plasmids. To generate GFP-Rheb-ER, a cDNA (IDT, Coralville, IA) containing a fragment of Cytochrome b5 (region from amino acids 95-134 (Itakura and Mizushima, 2010) with myc tag and glycosylation site (Honsho et al., 1998) was cloned into GFP-Rheb$^{\Delta CAAX}$ (linearized at the C Terminus via PCR) by Gibson Assembly. Full length RhebL1 cDNA was synthesized (IDT) and cloned into *SmaI*-digested pEGFPC1 by Gibson Assembly. The following plasmids were kind gifts: LAMP1-mCherry from J. Lippincott-Schwartz (Janelia Research Campus, Ashburn, VA) and mRFP-Sec61B from T. Rapoport (Harvard University, Cambridge, MA). Oligonucleotide primers and cDNA sequences used to generate these plasmids are listed in Table S1.

Small guide RNAs (gRNAs) were designed using the CRISPR design tool (crispr.mit.edu) or selected from predesigned gRNA sequences (Sanjana et al., 2014). The gRNA-encoding DNA oligonucleotides (IDT) sequences were annealed and ligated into Bbs1-digested pX459 V2.0 plasmid that was provided by F. Zhang (Massachusetts Institute of Technology, Cambridge, MA) via Addgene (#62988, (Ran et al., 2013)) and transformed into Stabl3-competent *Escherichia coli* cells. The gRNA sequences are listed in Table S2.

Immunoblotting

Cells were lysed in Tris-Buffered Saline + 1% Triton X-100 (TBST) with protease and phosphatase inhibitor cocktails (Roche Diagnostics, Florham Park, NJ). To remove insoluble materials, lysates were centrifuged for 6 minutes at 14,000 rpm. Lysate protein

concentrations were measured via Bradford assay prior to denaturation with Laemmli buffer and 5-minutes at 95C. Immunoblotting was performed with 4-15% gradient Mini-PROTEAN TGX precast polyacrylamide gels and nitrocellulose membranes (Bio-Rad, Hercules, CA). Membranes were blocked with 5% milk in TBS with 0.1% Tween 20 (TBST) buffer and then incubated with antibodies in 5% milk or bovine serum albumin in TBST. Antibodies used in this study are summarized in the Table S4. Horseradish peroxidase signal detection was performed using chemiluminescent detection reagents (ThermoScientific) and the Versadoc imaging station (Bio-Rad). ImageJ (National Institutes of Health) was used to analyze the results and measure band intensities.

Cell Fractionation

To perform cell fractionation, 2 million HeLa cells were plated in 10-cm dishes. Cells were rinsed, scraped into chilled PBS, and spun at 1000 rpm for 10 minutes. PBS was aspirated and cells were resuspended in homogenization buffer (HB; 5 mM Tris-HCl, 250 mM sucrose, 1 mM egtazic acid (EGTA), pH 7.4) with protease and phosphatase inhibitor cocktails. Cells were homogenized using a ball-bearing cell cracker (20 passages at 10 μm clearance, Isobiotec, Germany). Lysates were centrifuged at 1000 rpm for 10 minutes to remove unlysed cells. Supernatent was spun at 45,000 rpm for 1 hour to pellet membrane. Supernatant containing cytosolic proteins and the re-suspended membrane pellet were analyzed via immunoblotting.

Immunofluorescence and Microscopy

Cells were grown on 12-mm No. 1 glass coverslips (Carolina Biological Supply) and fixed with 4% paraformaldehyde (PFA; Electron Microscopy Sciences, Hatfield, PA) in 0.1M sodium phosphate buffer (pH 7.2) for 30 minutes. To best preserve cell structure,

this was achieved by adding 8% PFA dropwise to cells growing on coverslips in growth medium. Coverslips were washed in PBS before permeabilization in PBS + 0.2% Triton X-100 for 10 minutes. Coverslips were blocked for 30 minutes in blocking buffer (5% NDS/PBS/0.2% Triton X-100). Cells were incubated in primary antibody overnight at 4°C in blocking buffer. Cells were subsequently washed 3x with 0.2% Triton X-100 and incubated in secondary antibody in blocking buffer for thirty minutes at room temperature. Cells were washed 3x with 0.2% Triton X-100 before preparing slides with Prolong Gold Mounting media (Invitrogen, Carlsbad, CA). Antibodies used in this study are summarized in the Table S4.

For live cell imaging, cells were grown on glass bottom dishes (MatTek Corporation, Ashland, MA) prior to imaging. Sub-confluent dishes were imaged via spinning disc confocal microscopy at room temperature in a buffer that contained: 136 mM NaCl, 2.5 mM KCl, 2 mM $CaCl_2$, 1.3 mM $MgCl_2$ and 10 mM Hepes, 0.2% Glucose, 0.2% BSA pH 7.4 (Brown et al., 2000). Dextran Alexa Fluor 647 (Invitrogen, #22914) was applied overnight and washed out one hour before imaging. Our microscope consisted of the UltraVIEW VOX system (PerkinElmer, Waltham, MA) including the Ti-R Eclipse, Nikon inverted microscope (equipped with a 60x CFI Plan Apo VC, NA 1.4, oil immersion), a spinning disk confocal scan head (CSU-X1, Yokogawa) and Volocity (PerkinElmer) software. Images were acquired without binning with a 14-bit (1,000 x 1,000) EMCCD (Hamamatsu Photonics) and processed with ImageJ. ImageJ JACoP plug-in was used to generate correlation coefficients (Bolte and Cordelieres, 2006).

CRISPR/Cas9 Genome Editing

Similar to a previously described protocol (Amick et al., 2018), to generate knock out cells, HeLa cells were co-transfected with Rheb and RhebL1 sgRNAs encoded within

the pX459 plasmid. On the next day, puromycin (2 µg/ml) was added and cells were selected for 2 days. Surviving cells were plated at single-cell density and allowed to recover. Putative knockout colonies were initially identified via immunoblotting and subsequently confirmed by sequencing of the genomic loci. To obtain genomic DNA sequence for the target site in the Rheb gene, DNA was extracted (QuickExtract DNA extraction solution; Epicentre Biotechnologies), the region of interest was amplified by PCR (primers summarized in Table S3), PCR products were cloned into the pCR-Blunt TOPO vector (Zero Blunt TOPO PCR cloning kit; ThermoFisher Scientific), and transformed into XL-1 Blue Supercompetent Cells (Agilent Technologies, Santa Clara, CA). Plasmid DNA was isolated from multiple colonies and sequenced.

To insert a 2xHA epitope tag at the endogenous Rheb locus, we utilized a CRISPR/Cas9 genome-editing system strategy as previously described (Amick et al., 2016; Leonetti et al., 2016; Petit et al., 2013; Richardson et al., 2016). The crRNA, tracr RNA and ssDNA oligo were resuspended in nuclease-free duplex buffer (IDT) to 100 µM. To form the RNA duplex, the crRNA and tracrRNA were added at a 1:1 ratio and heated for 5 min at 95°C, then cooled to room temperature. The RNA duplex (150 pmol), Cas9 (150 pmol) and OptiMem were mixed in a sterile tube and incubated for 10 minutes at room temperature to form RNP complex. Hela cells (750,000 cells) were electroporated (Cell Line Kit V, electroporation program Q01; Lonza, Basel, Switzerland) with 10 µl RNP complex crRNA and single-stranded DNA (ssDNA) repair template (IDT Ultramer format). Sequences are provided in Table S2. Clonal cell lines were generated and validated using western blotting and immunofluorescence.

Statistical Analysis

Data were analyzed using Prism (Graphpad software) and tests are denoted in figure legends. All error bars represent standard deviations. Data distribution was assumed to be normal, but this was not formally tested.

References

Amick, J., A. Roczniak-Ferguson, and S.M. Ferguson. 2016. C9orf72 binds SMCR8, localizes to lysosomes, and regulates mTORC1 signaling. *Mol Biol Cell*. 27:3040-3051.

Amick, J., A.K. Tharkeshwar, C. Amaya, and S.M. Ferguson. 2018. WDR41 supports lysosomal response to changes in amino acid availability. *Mol Biol Cell*. 29:2213-2227.

Ben-Sahra, I., and B.D. Manning. 2017. mTORC1 signaling and the metabolic control of cell growth. *Curr Opin Cell Biol*. 45:72-82.

Bolte, S., and F.P. Cordelieres. 2006. A guided tour into subcellular colocalization analysis in light microscopy. *J Microsc*. 224:213-232.

Brown, P.S., E. Wang, B. Aroeti, S.J. Chapin, K.E. Mostov, and K.W. Dunn. 2000. Definition of distinct compartments in polarized Madin-Darby canine kidney (MDCK) cells for membrane-volume sorting, polarized sorting and apical recycling. *Traffic*. 1:124-140.

Choy, E., V.K. Chiu, J. Silletti, M. Feoktistov, T. Morimoto, D. Michaelson, I.E. Ivanov, and M.R. Philips. 1999. Endomembrane trafficking of ras: the CAAX motif targets proteins to the ER and Golgi. *Cell*. 98:69-80.

Clark, G.J., M.S. Kinch, K. Rogers-Graham, S.M. Sebti, A.D. Hamilton, and C.J. Der. 1997. The Ras-related protein Rheb is farnesylated and antagonizes Ras signaling and transformation. *J Biol Chem*. 272:10608-10615.

Ferguson, S.M. 2015. Beyond indigestion: emerging roles for lysosome-based signaling in human disease. *Curr Opin Cell Biol*. 35:59-68.

Gonzalez, A., and M.N. Hall. 2017. Nutrient sensing and TOR signaling in yeast and mammals. *EMBO J*. 36:397-408.

Hancock, J.F., H. Paterson, and C.J. Marshall. 1990. A polybasic domain or palmitoylation is required in addition to the CAAX motif to localize p21ras to the plasma membrane. *Cell*. 63:133-139.

Hao, F., K. Kondo, T. Itoh, S. Ikari, S. Nada, M. Okada, and T. Noda. 2018. Rheb localized on the Golgi membrane activates lysosome-localized mTORC1 at the Golgi-lysosome contact site. *J Cell Sci*. 131.

Honsho, M., J.Y. Mitoma, and A. Ito. 1998. Retention of cytochrome b5 in the endoplasmic reticulum is transmembrane and luminal domain-dependent. *J Biol Chem*. 273:20860-20866.

Ismail, S.A., Y.X. Chen, A. Rusinova, A. Chandra, M. Bierbaum, L. Gremer, G. Triola, H. Waldmann, P.I. Bastiaens, and A. Wittinghofer. 2011. Arl2-GTP and Arl3-GTP regulate a GDI-like transport system for farnesylated cargo. *Nat Chem Biol*. 7:942-949.

Itakura, E., and N. Mizushima. 2010. Characterization of autophagosome formation site by a hierarchical analysis of mammalian Atg proteins. *Autophagy*. 6:764-776.

Leonetti, M.D., S. Sekine, D. Kamiyama, J.S. Weissman, and B. Huang. 2016. A scalable strategy for high-throughput GFP tagging of endogenous human proteins. *Proc Natl Acad Sci U S A*. 113:E3501-3508.

Menon, S., C.C. Dibble, G. Talbott, G. Hoxhaj, A.J. Valvezan, H. Takahashi, L.C. Cantley, and B.D. Manning. 2014. Spatial control of the TSC complex integrates insulin and nutrient regulation of mTORC1 at the lysosome. *Cell*. 156:771-785.

Petit, C.S., A. Roczniak-Ferguson, and S.M. Ferguson. 2013. Recruitment of folliculin to lysosomes supports the amino acid-dependent activation of Rag GTPases. *J Cell Biol*. 202:1107-1122.

Ran, F.A., P.D. Hsu, J. Wright, V. Agarwala, D.A. Scott, and F. Zhang. 2013. Genome engineering using the CRISPR-Cas9 system. *Nat Protoc*. 8:2281-2308.

Richardson, C.D., G.J. Ray, M.A. DeWitt, G.L. Curie, and J.E. Corn. 2016. Enhancing homology-directed genome editing by catalytically active and inactive CRISPR-Cas9 using asymmetric donor DNA. *Nat Biotechnol*. 34:339-344.

Rocks, O., A. Peyker, M. Kahms, P.J. Verveer, C. Koerner, M. Lumbierres, J. Kuhlmann, H. Waldmann, A. Wittinghofer, and P.I. Bastiaens. 2005. An acylation cycle regulates localization and activity of palmitoylated Ras isoforms. *Science*. 307:1746-1752.

Rowland, A.A., P.J. Chitwood, M.J. Phillips, and G.K. Voeltz. 2014. ER contact sites define the position and timing of endosome fission. *Cell*. 159:1027-1041.

Sancak, Y., L. Bar-Peled, R. Zoncu, A.L. Markhard, S. Nada, and D.M. Sabatini. 2010. Ragulator-Rag complex targets mTORC1 to the lysosomal surface and is necessary for its activation by amino acids. *Cell*. 141:290-303.

Sancak, Y., T.R. Peterson, Y.D. Shaul, R.A. Lindquist, C.C. Thoreen, L. Bar-Peled, and D.M. Sabatini. 2008. The Rag GTPases bind raptor and mediate amino acid signaling to mTORC1. *Science*. 320:1496-1501.

Sancak, Y., C.C. Thoreen, T.R. Peterson, R.A. Lindquist, S.A. Kang, E. Spooner, S.A. Carr, and D.M. Sabatini. 2007. PRAS40 is an insulin-regulated inhibitor of the mTORC1 protein kinase. *Mol Cell*. 25:903-915.

Sanjana, N.E., O. Shalem, and F. Zhang. 2014. Improved vectors and genome-wide libraries for CRISPR screening. *Nat Methods*. 11:783-784.

Sato, T., A. Nakashima, L. Guo, and F. Tamanoi. 2009. Specific activation of mTORC1 by Rheb G-protein in vitro involves enhanced recruitment of its substrate protein. *J Biol Chem*. 284:12783-12791.

Saxton, R.A., and D.M. Sabatini. 2017. mTOR Signaling in Growth, Metabolism, and Disease. *Cell*. 168:960-976.

Silvius, J.R., P. Bhagatji, R. Leventis, and D. Terrone. 2006. K-ras4B and prenylated proteins lacking "second signals" associate dynamically with cellular membranes. *Mol Biol Cell*. 17:192-202.

Silvius, J.R., and F. l'Heureux. 1994. Fluorimetric evaluation of the affinities of isoprenylated peptides for lipid bilayers. *Biochemistry*. 33:3014-3022.

Takahashi, K., M. Nakagawa, S.G. Young, and S. Yamanaka. 2005. Differential membrane localization of ERas and Rheb, two Ras-related proteins involved in the phosphatidylinositol 3-kinase/mTOR pathway. *J Biol Chem*. 280:32768-32774.

Walton, Z.E., C.H. Patel, R.C. Brooks, Y. Yu, A. Ibrahim-Hashim, M. Riddle, A. Porcu, T. Jiang, B.L. Ecker, F. Tameire, C. Koumenis, A.T. Weeraratna, D.K. Welsh, R. Gillies, J.C. Alwine, L. Zhang, J.D. Powell, and C.V. Dang. 2018. Acid Suspends the Circadian Clock in Hypoxia through Inhibition of mTOR. *Cell*. 174:72-87 e32.

Yang, H., X. Jiang, B. Li, H.J. Yang, M. Miller, A. Yang, A. Dhar, and N.P. Pavletich. 2017. Mechanisms of mTORC1 activation by RHEB and inhibition by PRAS40. *Nature*. 552:368-373.

Zimmermann, G., B. Papke, S. Ismail, N. Vartak, A. Chandra, M. Hoffmann, S.A. Hahn, G. Triola, A. Wittinghofer, P.I. Bastiaens, and H. Waldmann. 2013. Small molecule inhibition of the KRAS-PDEdelta interaction impairs oncogenic KRAS signalling. *Nature*. 497:638-642.

Figure 1

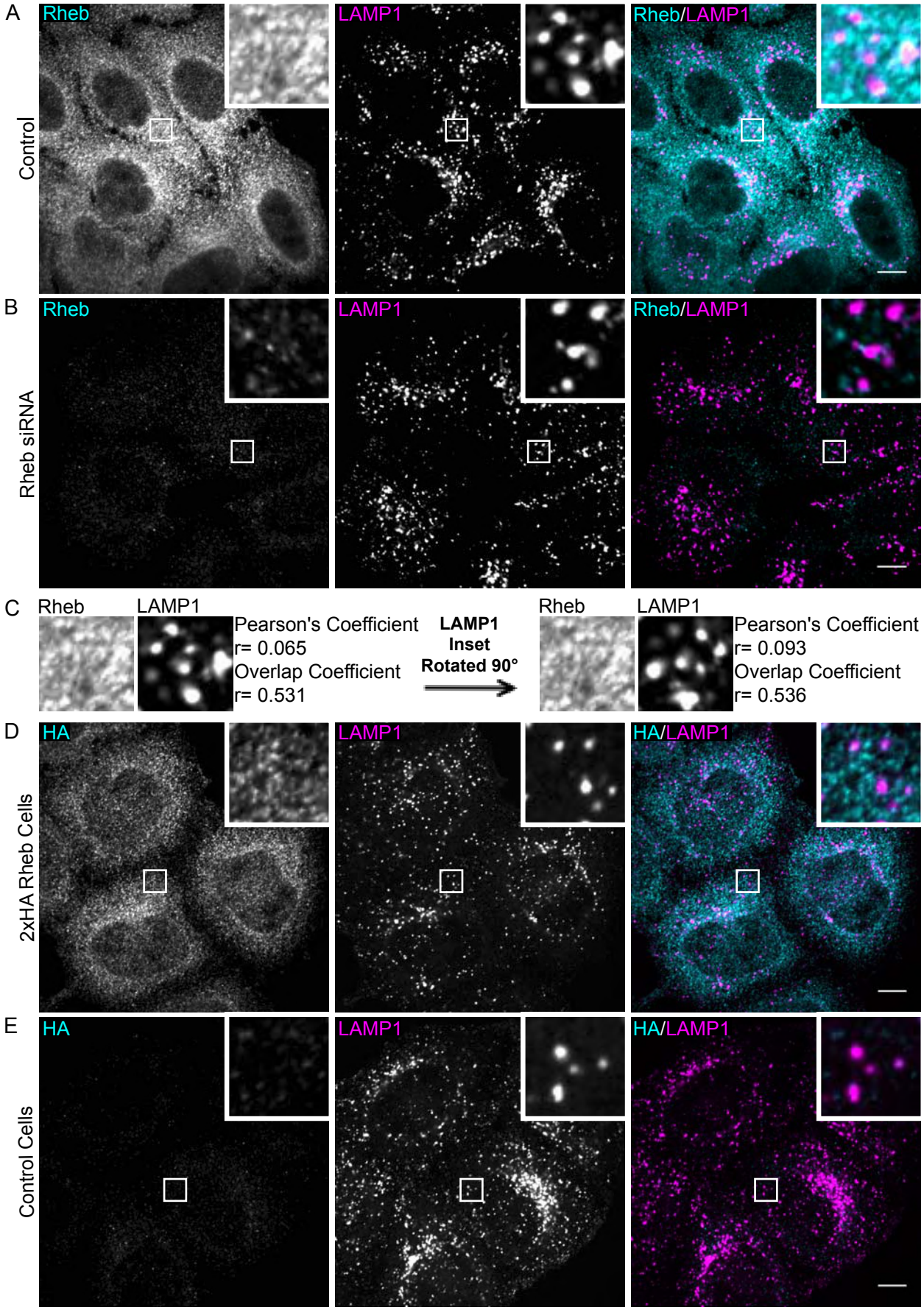

Figure 1. Rheb is not enriched on lysosomes. (A and B) Rheb and LAMP1 (late endosomes/lysosomes) immunofluorescence in HeLa cells that were transfected with control and Rheb siRNA respectively. **(C)** Correlation coefficients for Rheb and Lamp1 colocalization in the insets from panel A were calculated before and after rotating the LAMP1 inset by 90°.
(D and E) Immunofluorescence images of anti-HA and anti-LAMP1 staining in CRISPR-edited 2xHA-Rheb HeLa cells and control HeLa cells respectively. Scale bars, 10 μm.

Figure 2

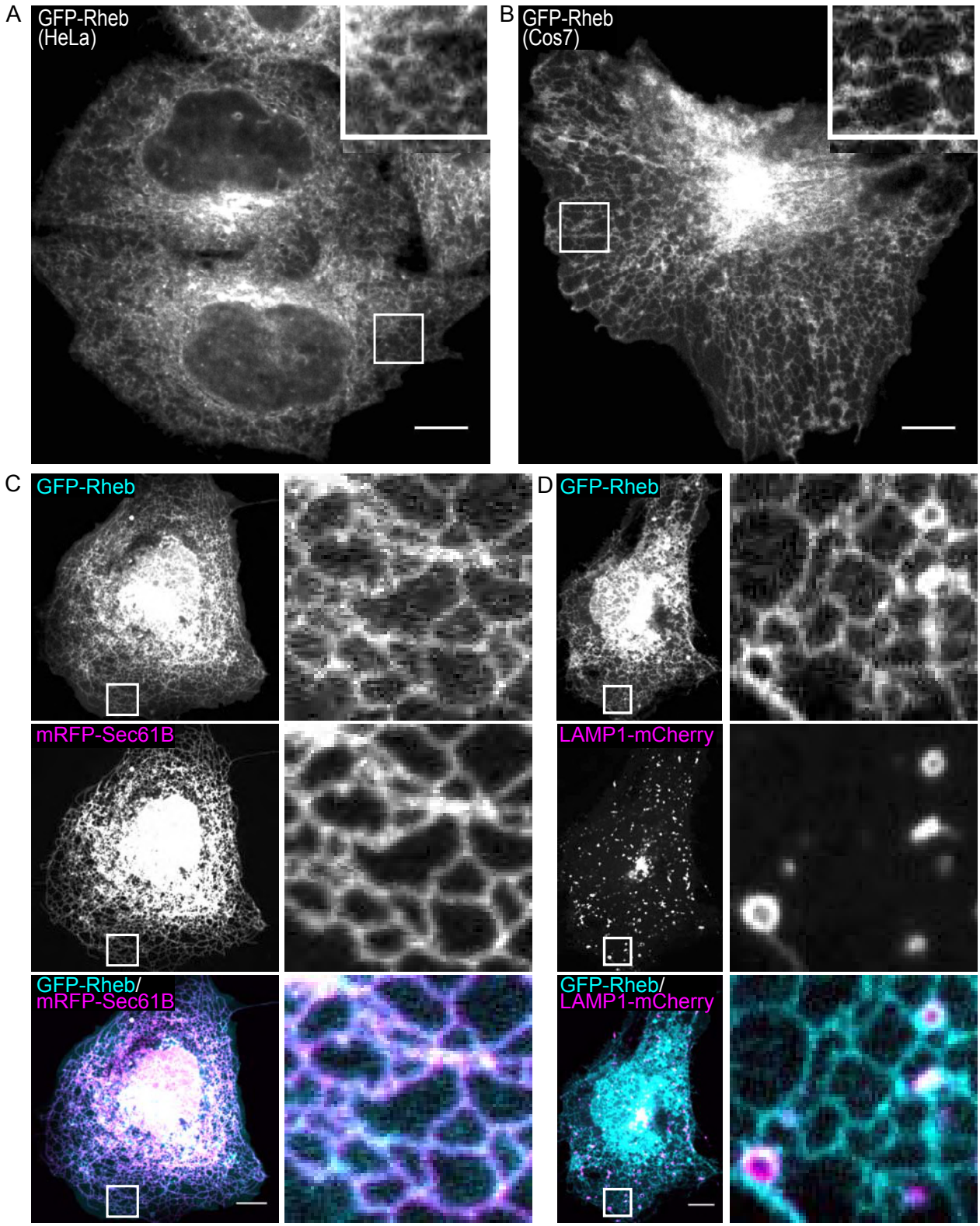

Figure 2. GFP-Rheb localizes to the ER and cytosol. (A and B) Spinning disk confocal live-cell imaging of GFP-Rheb in HeLa cells and COS-7 cells respectively. **(C)** GFP-Rheb and mRFP-Sec61B (ER marker) localization in COS-7 cells. **(D)** GFP-Rheb and LAMP1-mCherry (late endosomes and lysosomes) localization in COS-7 cells. Scale bars, 10 μm.

Figure 3

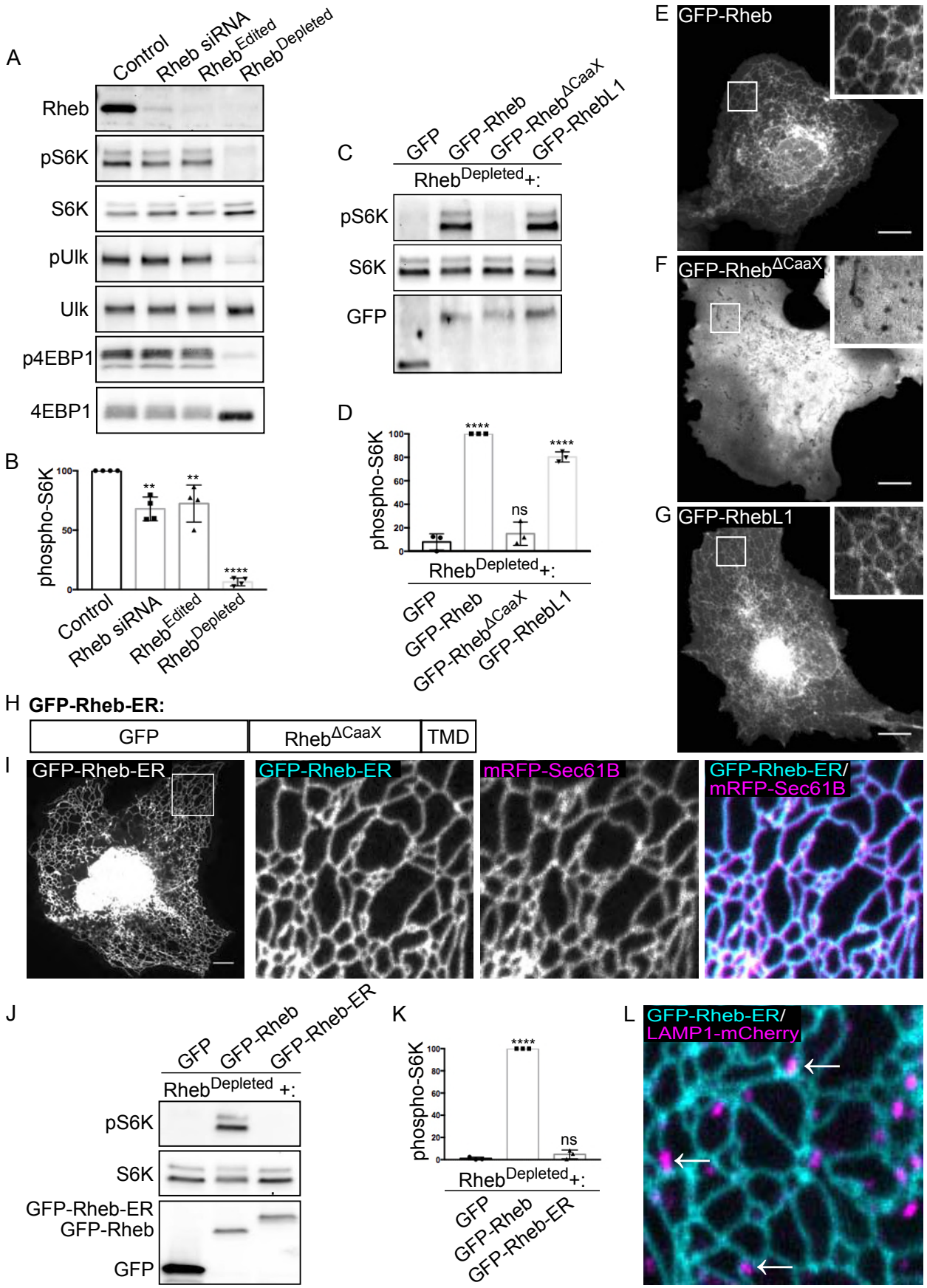

Figure 3. Farnesylation-dependent membrane interactions are critical for Rheb function. **(A)** Immunoblot analysis of Rheb levels and phosphorylation status of mTORC1 substrates (pS6K, Ulk, and 4EBP1) in Control, Rheb siRNA-treated, $Rheb^{Edited}$ (Rheb hypomorph+RhebL1 KO), and $Rheb^{Depleted}$ (Rheb hypomorph+RhebL1 KO+Rheb siRNA) HeLa cells. **(B)** Quantification of phospho-S6K levels under the indicated conditions where phospho-S6K levels were divided by S6K and normalized to Control (**, P<0.01; ****, P<0.0001; ANOVA with Dunnett's Multiple Comparisons Test, n=4). **(C)** Immunoblot analysis of phospho-S6K levels in $Rheb^{Depleted}$ cells transfected with the indicated plasmids. **(D)** Quantification of phospho-S6K levels from panel C. The phospho-S6K levels were divided by S6K and GFP values to control for loading and transfection efficiency. Values were normalized to GFP-Rheb. Statistics were calculated in comparison to the GFP transfection. (****, P<0.0001; ANOVA with Dunnett's Multiple Comparisons Test; n=3). **(E, F, G)** Live-cell images of GFP-Rheb, GFP-$Rheb^{\Delta CaaX}$, and GFP-RhebL1 in a COS-7 cells respectively. **(H)** Schematic of GFP-Rheb-ER chimera that contains N-terminal GFP, $Rheb^{\Delta CaaX}$, and the transmembrane domain of Cytochrome b5 (TMD). **(I)** Live-cell imaging of GFP-Rheb-ER localization. The leftmost image displays a low magnification view of GFP-Rheb-ER in a COS-7 cell. The three subsequent panels show higher magnifications of GFP-Rheb-ER and mRFP-Sec61B from the inset region. **(J)** Immunoblot analysis of phospho-S6K signaling in $Rheb^{Depleted}$ cells transfected with the indicated plasmids. **(K)** Quantification of phospho-S6K levels in panel I. The phospho-S6K levels were divided by S6K and GFP values to control for loading and transfection. Values were normalized to GFP-Rheb. Statistics were calculated in comparison to GFP (****, P<0.0001; ANOVA with Dunnett's Multiple Comparisons Test; n=3). **(L)** Image the spatial relationship between GFP-Rheb-ER on ER tubules and LAMP1-positive lysosomes. Scale bars, 10 μm.

Figure 4

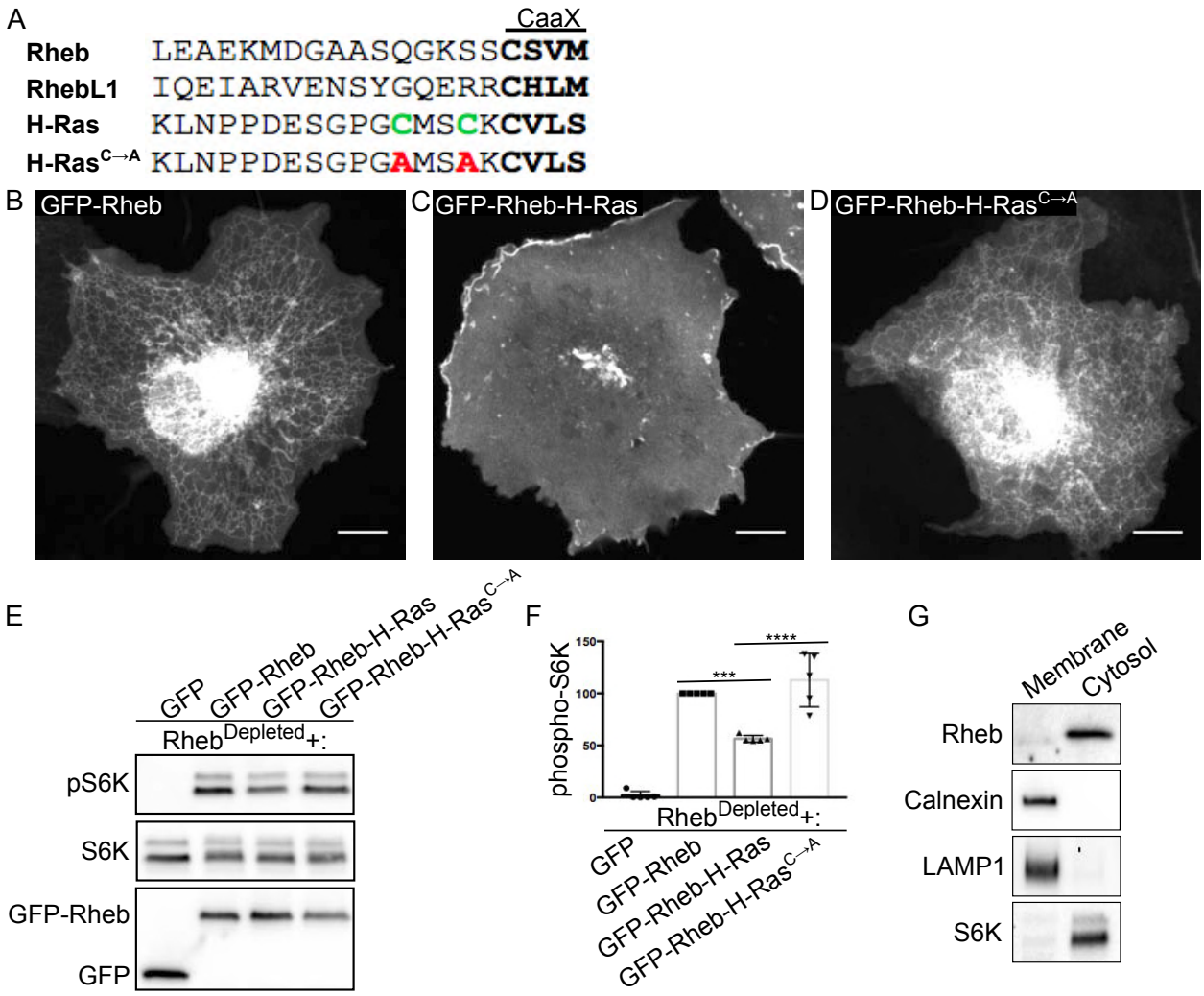

Figure 4. Rheb C-terminal farnesylation confers weak membrane interactions that are optimal for mTORC1 activation. (A) Alignment of the hypervariable regions of Rheb, RhebL1 and H-Ras proteins with CaaX motifs highlighted in bold and palmitoylated cysteines in green. These cysteines were mutated to alanines (red) in the GFP-Rheb-HRas$^{C\rightarrow A}$ mutant. **(B-D)** Live-cell images of GFP-Rheb, GFP-Rheb-HRas and GFP-Rheb-HRas$^{C\rightarrow A}$ in COS-7 cells respectively. **(E)** Immunoblot analysis of phospho-S6K levels in Rheb^{Depleted} cells transfected with the indicated plasmids. **(F)** Quantification of phospho-S6K levels from panel E. Phospho-S6K levels were divided by S6K and GFP values to control for loading and transfection and then normalized to GFP-Rheb. Statistics were calculated in comparison to GFP-Rheb-HRas. (***, P<0.001; ****, P<0.0001; ANOVA with Tukey's Multiple Comparisons Test; n=5). **(G)** Immunoblot analysis of proteins identified in membrane and cytosolic fractions of HeLa cells. Scale bars, 10 μm.

Supplemental Figure 1

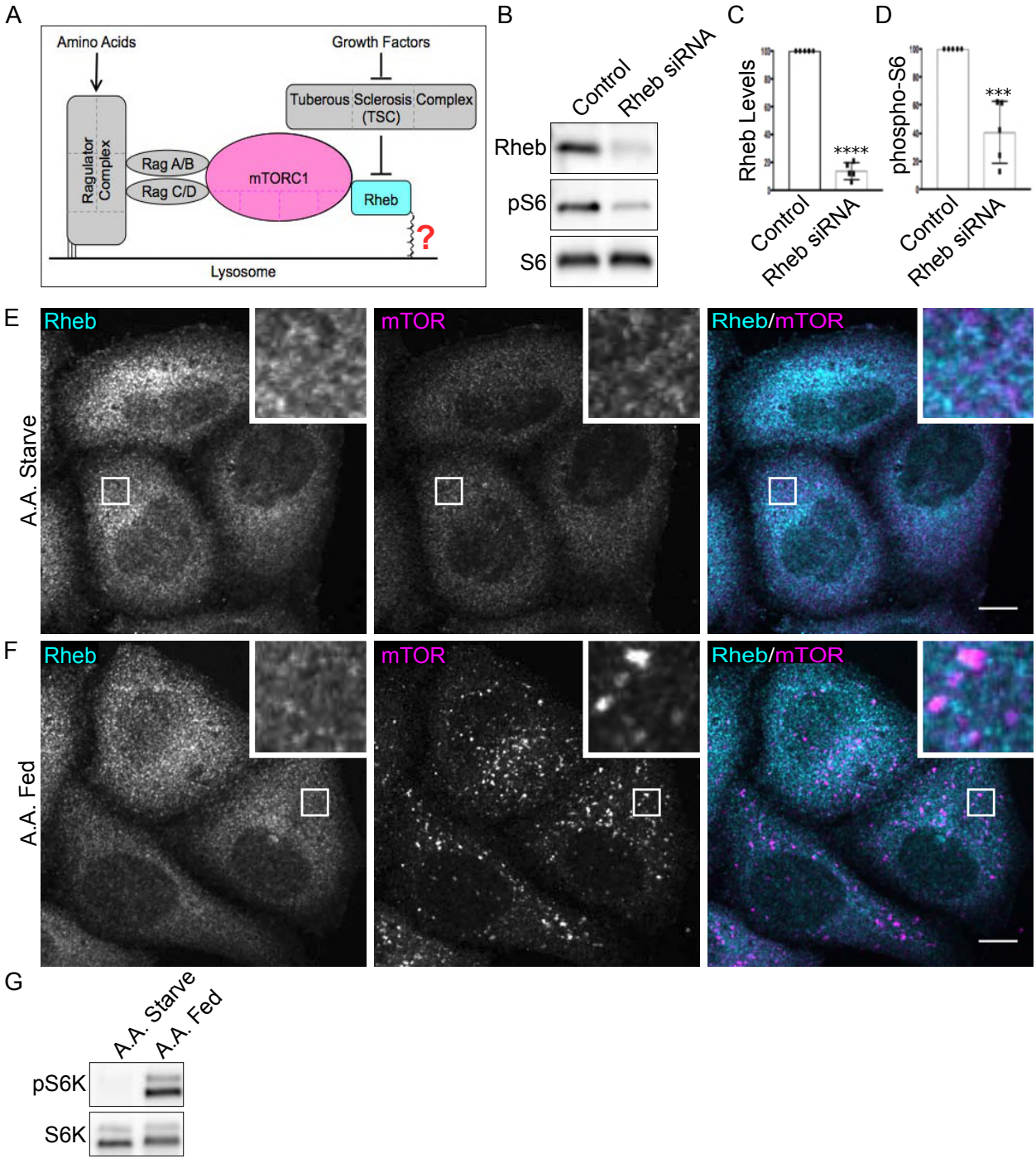

Supplemental Figure 1. Subcellular localization of Rheb is not responsive to amino acid availability. (A) Schematic diagram depicting the widely accepted model for mTORC1 activation on the surface of lysosomes. **(B)** Immunoblot analysis of Control and Rheb siRNA-treated HeLa cells. **(C)** Quantification of Rheb protein levels in Control and Rheb siRNA-treated cells (****, P<0.0001; unpaired t-test; n=5). **(D)** Quantification of phospho-S6 levels in Control and Rheb siRNA-treated cells (***, P=0.0003; unpaired t-test; n=5). **(E)** Representative immunofluorescence images of Rheb and mTOR localization in HeLa cells after a 2-hour amino acid (A.A) starvation. **(F)** Representative immunofluorescence images of mTOR and Rheb localization in HeLa cells following 20-minute A.A. refeeding of starved cells. **(G)** Immunoblot analysis of phospho-S6K and S6K levels in starved and re-fed HeLa cells. Scale bars, 10 μm.

Supplemental Figure 2

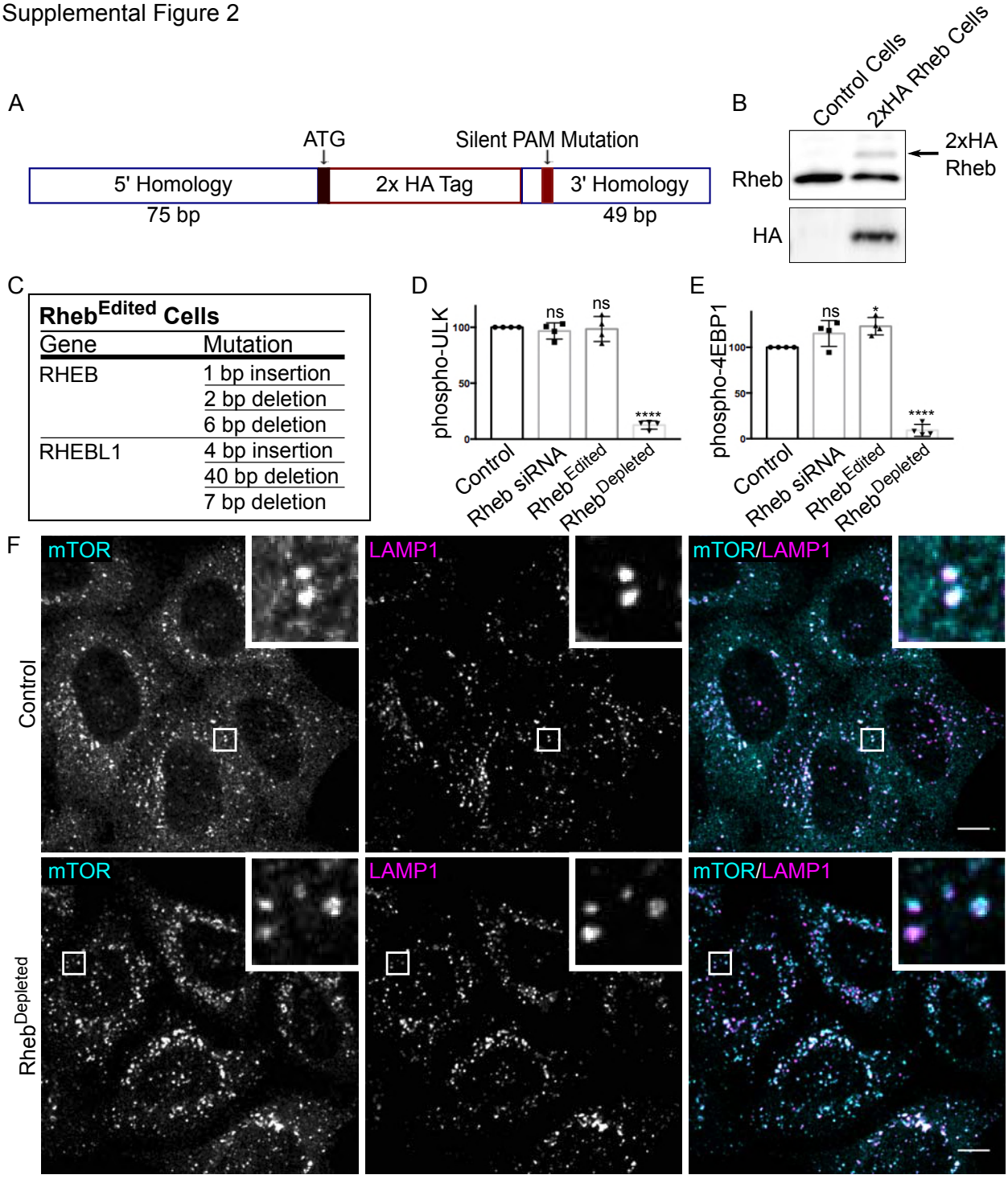

Supplemental Figure 2. Characterization of CRISPR-edited Rheb and RhebL1 mutant cells. (A) Summary of the genome editing strategy to used to insert a 2xHA epitope tag into the endogenous Rheb locus. **(B)** Western blot analysis of Control HeLa cells and 2xHA Rheb HeLa cells with anti-HA and anti-Rheb antibodies. **(C)** Summary of CRISPR-Cas9 mediated indels in $Rheb^{Edited}$/$Rheb^{Depleted}$ cells identified by sequencing of genomic DNA. **(D)** Quantification of phospho-Ulk in Control and Rheb siRNA-treated, $Rheb^{Edited}$, and $Rheb^{Depleted}$ HeLa cells (from Figure 3A). The phospho-Ulk levels were divided by Ulk and normalized to Control (****, P<0.0001; ANOVA with Dunnett's Multiple Comparisons Test, n=4). **(E)** Quantification of phospho-4EBP1 in Control and Rheb siRNA-treated, $Rheb^{Edited}$, and $Rheb^{Depleted}$ HeLa cells (from Figure 3A). phospho-4EBP1 levels were divided by 4EBP1 and normalized to Control (*, P<0.05; ****, P<0.0001; ANOVA with Dunnett's Multiple Comparisons Test, n=4). **(F)** Immunofluorescence images of the subcellular localization of mTOR and LAMP1 in control and $Rheb^{Depleted}$ HeLa cells. Scale bars, 10 μm.

Supplemental Figure 3

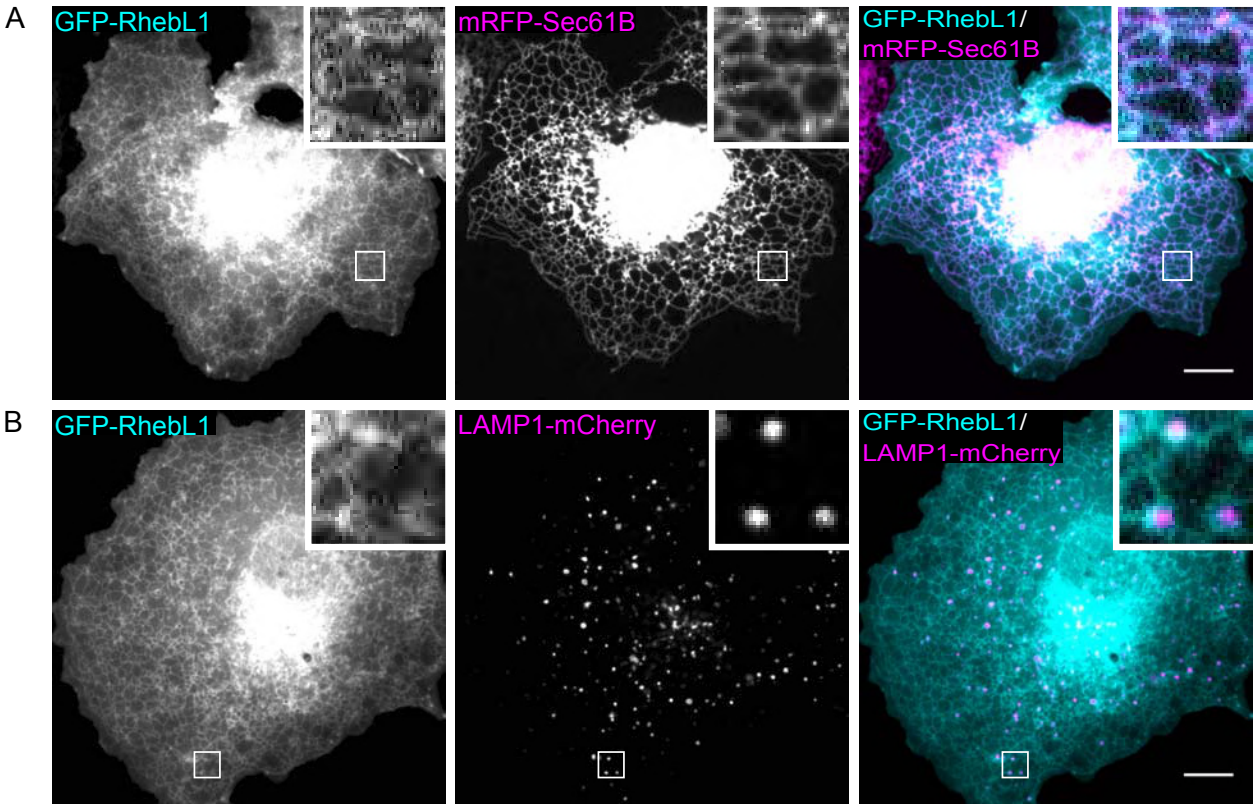

Supplemental Figure 3. GFP-RhebL1 localizes to ER and Cytosol. (A) GFP-RhebL1 and mRFP-Sec61B sub-cellular localization in COS-7 cells. **(B)** GFP-RhebL1 and LAMP1-mCherry sub-cellular localization. Scale bars, 10 μm.

Supplemental Figure 4

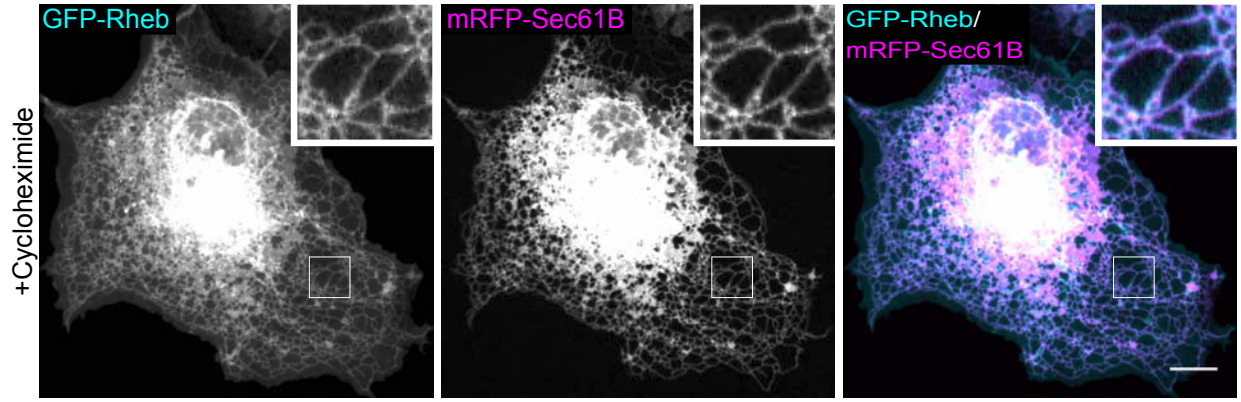

Supplemental Figure 4. ER localization of GFP-Rheb is not sensitive to inhibition of new protein synthesis. Live-cell imaging of GFP-Rheb localization following a 2 hour treatment of COS-7 cells with cycloheximide (100 µg/mL). Scale bar, 10 µm.

Supplemental Movie 1. GFP-Rheb localizes to dynamic ER tubules that contact lysosomes. Spinning disk confocal live-cell imaging of GFP-Rheb (cyan) and Dextran-loaded lysosomes (magenta; cells were labeled overnight with Alexa647-Dextran and washed for 1 hour before imaging). Images were acquired at a rate of 15 frames/minute over an interval of 5 minutes. Scale bar, 5 μm.

Table S1: Summary of Oligonucleotides used in Plasmid Construction

Target	Use	Sequence (5'-3')
Rheb Forward	Rheb forward primer for cloning into pEGFP-C1	**CAGTCGACGGTACCGCGGGCCC**aATGCC GCAGTCCAAGTCCCGGA
Rheb Reverse	Rheb reverse primer for cloning into into pEGFP-C1	**CAGTTATCTAGATCCGGTGGATCCC**TCA CATCACCGAGCACGAA
Rheb^{CaaX} Forward	Site directed mutagenesis (SDM) forward primer to delete Rheb CaaX box	TGAGGGATCCACCGGATC
Rheb^{CaaX} Reverse	SDM reverse primer to delete Rheb CaaX box	CGAAGACTTCCCTTGTGAAG
Rheb-H-Ras Forward	SDM forward primer to replace Rheb hypervariable region (HVR) with HRas HVR	ctgcatgagctgcaagtgtgtgctctcctgaGGGATCCA CCGGATCTAG
Rheb-H-Ras Reverse	SDM reverse primer to replace Rheb HVR with H-Ras HVR	ccggggccactctcatcaggagggttcagcttTTTTTCT GCCTCCAAAATTATCC
Rheb-H-Ras$^{C\rightarrow A}$ Forward	SDM forward primer to mutate C to A in H-Ras HVR	agcgccAAGTGTGTGCTCTCCTGAGC
Rheb-H-Ras $^{C\rightarrow A}$ Reverse	SDM reverse primer to mutate C to A in H-Ras HVR	catggcGCCGGGGCCACTCTCATC
Cytochrome b5 cDNA	cDNA added to C Terminus of Rheb^{CaaX} to generate GFP-Rheb-ER	AGCTTCACAAGGGAAGTCTTCGccggaaact cttatcactactattgattctagttccagttggtggaccaactgg gtgatccctgccatctctgcagtggccgtcgccttgatgtatcg cctatacatggcagaggactgaGGGATCCACCGGA TCTAGATAA
RhebL1 cDNA	cDNA with overhangs to insert RhebL1 into pEGFP-C1	GCAGTCGACGGTACCGCGGGCCCaATGC CGCTAGTCCGCTACAGGAAGGTGGTCAT CCTCGGATACCGCTGTGTAGGGAAGACA TCTTTGGCACATCAATTTGTGGAAGGCGA GTTCTCGGAAGGCTACGATCCTACAGTG GAGAATACTTACAGCAAGATAGTGACTCT TGGCAAAGATGAGTTTCACCTACATCTGG TGGACACAGCAGGGCAGGATGAGTACAG CATTCTGCCCTATTCATTCATCATTGGGG TCCATGGTTATGTGCTTGTGTATTCTGTCA CCTCTCTGCATAGCTTCCAAGTCATTGAG AGTCTGTACCAAAAGCTACATGAAGGCCA TGGGAAAACCCGGGTGCCAGTGGTTCTA GTGGGGAACAAGGCAGATCTCTCTCCAG AGAGAGAGGTACAGGCAGTTGAAGGAAA GAAGCTGGCAGAGTCCTGGGGTGCGACA TTTATGGAGTCATCTGCTCGAGAGAATCA GCTGACTCAAGGCATCTTCACCAAAGTCA TCCAGGAGATTGCCCGTGTGGAGAATTC CTATGGGCAAGAGCGTCGCTGCCATCTC ATGTGAGGGATCCACCGGATCTAGATAAC

Table S2: Summary of Oligonucleotides for Gene-Editing Experiments

Gene	Use	Sense (5'-3')	Antisense (5'-3')
RHEB	gRNA for KO	CACCGCTACATAC CTTTCCATATGC	AAACGCATATGGA AAGGTATGTAGC
RHEBL1	gRNA for KO	CACCGATCCTCGG ATACCGCTGTGT	AAACACACAGCGG TATCCGAGGATC
RHEB	crRNA for 2xHA tag insertion	GAUCGCGAUCUUC CGGGACUGUUU UAGAGCUAUGCU	
RHEB	2xHA tag template	GCCGCCGATCACA GCAGCAGGAGCCA CCGCCGCCGCGGT TGATGTGGTTGGG CCGGGGCTGAGGA GGCCGCCAAGATG tacccatacgatgttccaga ttacgcttatccctatgacgtc ccggactatgcaCCGCA GTCTAAGTCCCGG AAGATCGCGATCC TGGGCTACCGGTC TGTGG	

Table S3: Summary of Oligonucleotide Primers for PCR Amplification of Genomic DNA

Target	Sense (5'-3')	Antisense (5'-3')
RHEB	GTATCTTCTGAGCAATACAATC	ACCATAACACCTCTGAACGGAT
RHEBL1	ACTTTCCTGCACCAGCTGCCG	TTCCAATCCTCGCTCTACAAC

Table S4: Summary of Antibodies

Target Protein	**Source**	**Catalog No.**
4EBP1	Cell Signaling Technology	9644S
P-4EBP1 (T37/46)	Cell Signaling Technology	2855S
Anti-Rabbit, HRP	Cell Signaling Technology	7074S
Anti-Mouse, HRP	Cell Signaling Technology	7076S
Anti-biotin, HRP	Cell Signaling Technology	7075P5
Calnexin	Cell Signaling Technology	2679S
Donkey anti-Mouse, Alexa Fluor 488	Thermo Fischer Scientific	A21202
Donkey anti-Mouse, Alexa Fluor 594	Thermo Fischer Scientific	A21203
Donkey anti-Rabbit, Alexa Fluor 488	Thermo Fischer Scientific	A21206
Donkey anti-Mouse, Alexa Fluor 594	Thermo Fischer Scientific	A21207
GFP-HRP	Rockland	600-103-215
HA	Cell Signaling Technology	2367S
HA-HRP	Roche	12 013 819 001
LAMP1	DSHB	H4A3
LAMP1	Cell Signaling Technology	9091S
mTOR	Cell Signaling Technology	2983S
p70 S6K	Cell Signaling Technology	9202S
P-p70 S6K (T389)	Cell Signaling Technology	9234S
Rheb	Abnova	H00006009-M01
S6	Cell Signaling Technology	2217S
P-S6 (S235/236)	Cell Signaling Technology	4858S
ULK	Cell Signaling Technology	8054S
P-ULK (S757)	Cell Signaling Technology	14202S